

Lab on a Chip

Accepted Manuscript



This is an *Accepted Manuscript*, which has been through the Royal Society of Chemistry peer review process and has been accepted for publication.

Accepted Manuscripts are published online shortly after acceptance, before technical editing, formatting and proof reading. Using this free service, authors can make their results available to the community, in citable form, before we publish the edited article. We will replace this *Accepted Manuscript* with the edited and formatted *Advance Article* as soon as it is available.

You can find more information about *Accepted Manuscripts* in the [Information for Authors](#).

Please note that technical editing may introduce minor changes to the text and/or graphics, which may alter content. The journal's standard [Terms & Conditions](#) and the [Ethical guidelines](#) still apply. In no event shall the Royal Society of Chemistry be held responsible for any errors or omissions in this *Accepted Manuscript* or any consequences arising from the use of any information it contains.

Cite this: DOI: 10.1039/xxxxxxxxxx

On-chip phase measurement for microparticles trapped on a waveguide[†]

Firehun Tsige Dullo,^{*a,b} and Olav Gaute Hellesø^bReceived Date
Accepted Date

DOI: 10.1039/xxxxxxxxxx

www.rsc.org/journalname

Polystyrene microparticles are trapped on a waveguide Young interferometer and the phase change caused by the trapped particles is measured. This is a novel, on-chip method that can be used to count and characterize trapped particles. The trapping of single particles is clearly identified. Simulations show that the phase change increases with the diameter upto 7 μm , while for larger particles, morphology-dependent resonances appear. For 7 μm particles, a phase change of -0.13 rad is measured, while the simulated value is -0.28 rad. Extensive simulations are carried out regarding the phase change, waveguide transmission and the forces on the particles, and also regarding sources of the discrepancy between simulations and measurements.

1 Introduction

Optical waveguides provide a set of optical functions that can be combined with other types of functions (optical, chemical, microfluidic and electronics) on the same chip. They are thus attractive devices for on-chip manipulation, detection and sorting of particles^{1–12}.

Optical waveguides have an evanescent field that stretches about 250 nm from their surfaces. When a particle solution is introduced on a waveguide surface, the particles interact with this field. As a result, the particles are pulled down to the waveguide surface and propelled forward by the strong gradient and radiation forces, respectively. This was first demonstrated in 1992 by Kawata and Sugiura¹. In addition to propulsion of various types of particles, several optical functions have been demonstrated. Microparticles have been trapped and held at a specific location with a waveguide loop with an intentional gap⁶. Nanoparticles can be stopped in a similar way, using a gold bowtie on top of the waveguide¹⁰. Recently, dielectric microparticles have been sorted according to size¹¹. The trapped particles are normally observed from above, using bright-field, dark-field or fluorescence microscopy. Raman-spectroscopy from above has also been demonstrated⁸. In order to have a lab-on-chip system, it is advantageous if on-chip methods can also be used to detect and characterize the trapped particles. A few on-chip detection methods have been demonstrated, including on-chip Raman-spectroscopy⁹ and measuring the change in resonance frequency of a photonic crystal⁷.

When a particle is trapped on a waveguide, it interacts with

the evanescent field of the waveguide. This gives a change in the phase and transmission of the guided light. Some light is also scattered back towards the input of the waveguide. Waveguide interferometers are commonly used for biological and chemical sensing applications^{13–15}. The most common Mach-Zehnder interferometer has a single-mode output waveguide, which makes it difficult to distinguish between changes in phase and amplitude. The Young interferometer has a set of interference fringes on the output^{16,17}. A phase change moves the interference fringes while decreased transmission of the device reduces the intensity of the fringes. With the Young interferometer, changes in phase can readily be separated from changes in amplitude. In this work, we have used a Young interferometer to study the phase change caused by trapping of a particle. Particles have been trapped on the surface of the waveguides constituting the two arms of the interferometer. The phase-change can potentially be used to detect and characterize the trapped particle, and it may also give information about the trapping process. To our knowledge, trapping on an interferometer has not been reported previously.

2 Methods

2.1 Waveguides and interferometer design

For the first works on waveguide trapping, waveguides made by ion-exchange were used^{1–3}, while subsequent studies have mainly used silicon nitride (Si_3N_4) waveguides^{4–6,8–11} due to the higher index contrast and thus larger optical forces. For this work, we thus chose to use Si_3N_4 waveguides on oxidized silicon substrates. Shallow rib waveguides were made by wet-etching a 5 nm high, 2 μm wide rib into a 150 nm thick Si_3N_4 core. The fabrication process is as detailed in¹³. The shallow rib ensures single-mode condition for relatively wide waveguides, while the thin core gives a strong evanescent field. The latter is a prerequi-

^a Northern Research Institute, 9294 Tromsø, Norway. E-mail: firehun.tsige.dullo@norut.no

^b Department of Physics and Technology, University of Tromsø, 9037 Tromsø, Norway.

site for efficient optical trapping and high sensitivity for the Young interferometer. The measured propagation loss of the waveguides was 0.8-1.3 dB/cm, partly depending on the top-cladding.

Fig. 1 shows the waveguide Young interferometer. An input optical waveguide is split in two waveguide arms by a symmetric Y-junction. The arms contain a sensing region each, as described in more detail below. Each arm has a sensing region, followed by a lateral expansion giving an inclined, tapered section. At the end, the tapers have an angle of 0.8° relative to the centre-line of the interferometer. Light emerges from the fundamental mode of the tapers, propagating into a planar waveguide, where an interference pattern is obtained. The 0.8° inclination gives good overlap between the beams, and thus interference fringes with high visibility will be obtained approximately 1 mm from the end of the tapers. When a polystyrene microparticle is trapped in one of the sensing regions, the refractive index is changed from that of water ($n = 1.33$) to that of polystyrene ($n = 1.59$). This gives a phase change for the waveguide mode, which causes the interference pattern to be displaced laterally.

During fabrication, the waveguide is covered with a $1\ \mu\text{m}$ thick top-cladding of silica. Sensing windows are made by wet-etching this silica-layer down to the Si_3N_4 core. The sensing windows were originally 20 mm long (designed for gas-sensing), but for this work the length was reduced to approximately 1 mm by depositing a layer of PDMS across the sensing windows. This made it possible to observe the entire sensing region with a 10x microscope objective, which is necessary to keep control of all trapped particles. The distance between the two arms of the interferometer was $25\ \mu\text{m}$. Note that the two arms of the interferometer are perfectly symmetric, with a 1 mm long sensing window on both arms. Thus, a particle should give a positive or a negative phase change according to which arm it is trapped on. Also, a perfectly symmetric Young interferometer gives high visibility of the interference fringes as losses will be the same for the two arms.

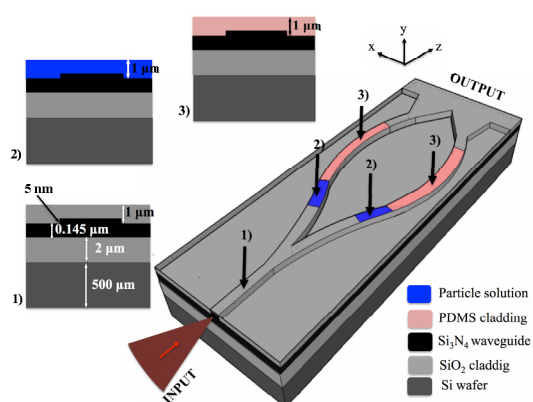


Fig. 1 Outline of the Young interferometer made with shallow rib waveguides. Both arms have a 20 mm long sensing window etched into the silica top-cladding. For this work, the length of the sensing windows was reduced to 1mm with a PDMS-layer, in order to see the entire openings with a microscope objective. The inserts show the cross-sections of 1) the silica cladded regions, 2) the particle solution regions and 3) the PDMS cladded regions

2.2 Experimental setup

Fig. 2 shows a schematic diagram of our experimental apparatus for optical trapping and detection of the resulting phase change. The laser is an Ytterbium fiber laser, with 1070 nm wavelength and the output power kept to 400 mW. The polarization was set with a half-wave plate to TE-polarization. Light was coupled into the waveguide by an objective lens (20x, 0.4 N.A, NIR Thorlabs). The waveguide chip was mounted on an aluminum plate. The temperature was stabilized at 23.5°C by a Peltier element to reduce temperature-induced noise in the interferometer. On top of the chip, a PDMS-chamber was used to contain the solution with microparticles. The microparticles could thus enter into the evanescent field of the waveguides, within the 1 mm long opening in the sensing windows. A microscope with a 10x objective and a CCD-camera was used to record movies of the trapped microparticles from above. The interference fringes at the output face of the chip were collected by a 10x objective and focused onto a camera, to record the interference fringes.

The microparticles were polystyrene spheres (Duke Scientific) with refractive index $n = 1.59$ and density $1.05\text{g}/\text{cm}^3$. According to the specifications for the spheres, the diameters and their standard deviations were $6.992 \pm 0.050\ \mu\text{m}$, $9.964 \pm 0.058\ \mu\text{m}$, $12.01 \pm 0.07\ \mu\text{m}$ and $15.02 \pm 0.08\ \mu\text{m}$.

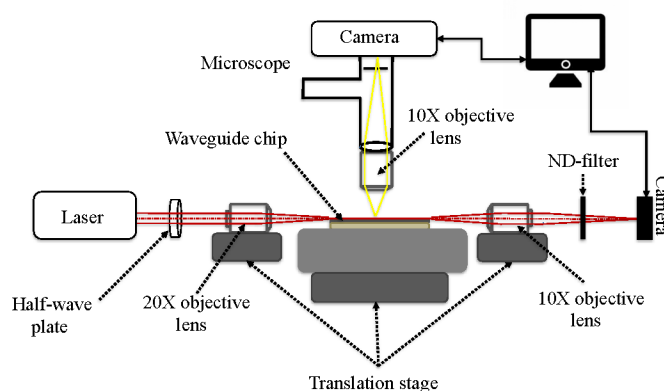


Fig. 2 Schematic diagram of the experimental set-up for optical trapping and detection of microparticles on waveguides.

2.3 Simulations

A commercial software (Comsol 5.1) based on the finite element method was used to simulate the phase change due to the presence of a microsphere on an optical waveguide. An example of the model is shown in Fig. 3. It consists of the under-cladding (silica), the waveguide core (silicon nitride), water and the sphere (polystyrene). In most cases, the sphere was positioned on the centre of the waveguide, making the model symmetric. Thus, to reduce the size, only half the problem was simulated as shown in Fig. 3. This was accomplished by setting the symmetry-plane to be a perfect electric conductor, and consequently doing the simulations for TE-polarization. The full model (not exploiting symmetry) gave the same results as half the model for the symmetric case. Perfectly matched layers (PML) were used before and after

the waveguide to avoid reflections. First, the fundamental mode of the waveguide was found, then the model was solved in three dimensions. As the rib of the waveguide is 5 nm and the diameter of the sphere up to 15 μm , the model is large. Thus, the 3D-model was run on a computer cluster. After finding the field distribution, the S-parameters were found for the input and output ends of the waveguide, with the complex value of S21 giving the phase and transmission. The backscattering into the waveguide is given by S11. Optical forces were calculated by integrating the Maxwell stress tensor over the surface of the sphere⁴.

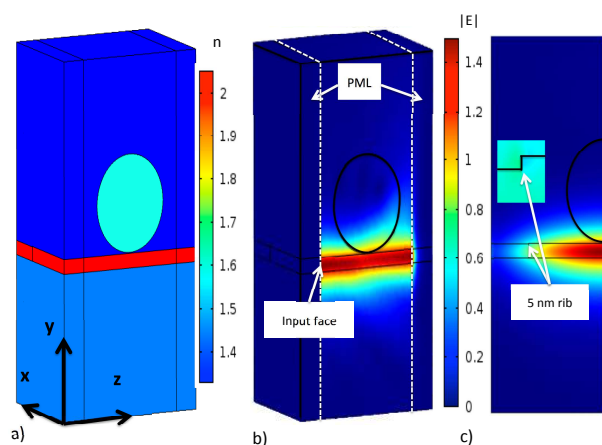


Fig. 3 Outline of the simulation model for a 1 μm sphere. a) Refractive indices of the materials. b) Field-distribution (norm of electrical field). The input and output faces are shown with white dashed lines, with PMLs before the input face and after the output face. c) Field-distribution on the input face with the rim of the sphere shown.

In order to find the phase change, the phase at the output of the waveguide (given by S21) was first calculated with the refractive index of the sphere set to 1.33, i.e. that of water. Then the calculation was repeated with the refractive index set to 1.59, i.e. that of polystyrene. The phase-change was taken to be the difference between the two calculated phases. It was thus sufficient to do the simulations for a single, straight waveguide, rather than for the two arms of the Young interferometer.

A fine mesh ($\lambda/5$ or $\lambda/7$) was used in the waveguide core and close to the surface of the sphere. In parts of the model with little or no light, a coarse mesh was used in order to limit the amount of memory required. The model was verified with various mesh settings and found to give consistent results. The transmission with a water-sphere was between 98.8 % and 100.2% at the output of the waveguide for all simulated sphere-sizes. The variation is due to numerical resolution, as a water-sphere in water, with zero absorption, ideally gives 100% transmission. The simulated backscattering from a water-sphere was approximately 0.5%. As the backscattering for a water-sphere in water should be zero, this corresponds to the numerical noise-level of the simulations. It was only resonances for large spheres ($> 12 \mu\text{m}$) that gave a backscattering larger than this noise-level. We have thus omitted backscattering from the results presented as simulations with higher precision are necessary to get reliable results.

The refractive indices used were 1.33 for water, 1.59 for polystyrene, 1.4496 for silica¹⁸ and 2.05 for silicon nitride¹⁹. However, other values are also given in the literature for these materials and for a wavelength of 1070 nm^{20,21}. Simulations are presented in the Results-section to check the influence of these material parameters, and in particular of the refractive index of the sphere.

2.4 Analysis of the interference pattern

As discussed above, the phase difference between the two arms of the interferometer create a lateral displacement of the interference pattern at the output. The intensity-distribution of the interference pattern is given by¹⁶:

$$I = I_{env} \cos^2\left(\frac{\varphi}{2} + kx \sin(\gamma)\right) \quad (1)$$

where φ is the phase difference between the two arms, γ is the angle of inclination between the tapered waveguides, x is the lateral position of the fringes and $k = nk_o = 2\pi n/\lambda_o$ is the wave number. The envelope function I_{env} depends on the taper width and, in our case of 25 μm wide tapers, limits the number of fringes to three. An example of three recorded fringes are shown in Fig. 4.

From eq. 1, the position y_i of the peak of fringe i is given by:

$$\frac{\varphi}{2} + kx_i \sin(\gamma) = i\pi, i = 0, \pm 1, \pm 2, \dots \quad (2)$$

By recording the positions x_i of the peaks of the fringes, eq. 2 can be solved for the two unknowns φ and $K = k \sin(\gamma)$. We have fitted gaussian functions to the intensity profile of the fringes and found the peak positions from the fitted functions. This gave precise and stable detection of the peak-positions and thus of the phase.

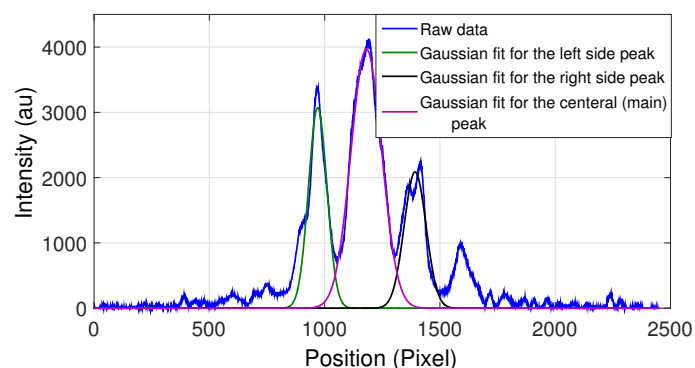


Fig. 4 Profile of the interference pattern along the x-direction.

3 Results and discussion

In Fig. 5 we have compared the output phase with the relative transmission (i.e. output power) as microparticles with 10, 12 and 15 μm diameter are trapped on the Young interferometer. The first particle is trapped at time 275 sec. on the left arm. Then a second particle is trapped at 400 sec. on the right arm. Finally, a third particle is trapped on the left arm. Particles were stably trapped and propelled along the waveguide until they reached

the PDMS-layer limiting the sensing window. Thus, particles did not leave the waveguide.

At 375 sec. the input power was slightly increased, creating a relatively large change in the transmission, while the corresponding change in phase is similar to the noise-level. This clearly demonstrates that the transmission is highly sensitive to the input coupling, while the phase is less influenced by this. In general, the noise relative to the change in signal due to trapping, is higher for transmission than for phase. Thus, phase change seems to be better for detection of trapped particles than amplitude-change. Both transmission and phase show a continuous drift as function of time, even though the interferometer is symmetric. Mechanical drift due to changes in room-temperature might change the input-coupling, and thus cause drift in the measured transmission. The most likely cause for phase-drift is the PDMS-layer that covers 19 out of the 20 mm total length of the sensing windows (see Fig. 1). As the input power was relatively high (400 mW), this PDMS-layer might absorb some light, giving temperature effects that influence the transmission and the phase. Fabrication imperfections may cause these effects to be different for the two arms. Absorption and temperature-effects are less likely when silica is used as top-cladding.

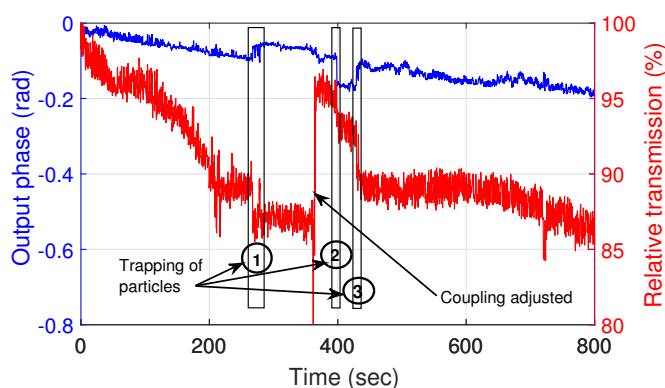


Fig. 5 Evidence of particle detection with output phase and relative transmission. Blue line shows the output phase (left y-axis) and red line shows relative transmission (right y-axis). The three rectangular boxes show the instants when particles get trapped, with particles 1 and 3 being trapped on the left arm (phase increases) and particle 2 on the right arm (phase decreases). The particles were stably trapped and propelled to the end of the sensing window.

Fig. 6a shows the output phase as a function of time for four trapping experiments with four different microparticle sizes. Trapping of a particle is seen to cause a step-like change of phase, with the sign of the step depending on trapping on the left or right arm of the interferometer. The step is larger for larger particles. After the initial step, there is some relatively large phase-fluctuations for 10 μm and 12 μm particles, that may indicate that the particle moves in and out of the evanescent field just after the initial trapping, and then gets firmly trapped. This is more visible in Fig. 6b, where two 12 μm particles are trapped successively. In both events, the particle appears to enter the evanescent field briefly, then re-enter and eventually ending up being stably trapped (not visible for second particle). The initial trapping depends on the trap stiffness and the microfluidic forces on the par-

ticle. In addition, it is possible that local surface roughness, flow in the water, direction and speed of approach can give interactions between the particle and the guided mode, causing the observed phase-fluctuations. The process seems to be random, with no dependency on the size of the particles. Due to the drift in the measured phase and the unstable phase right after trapping, we have, for subsequent measurements, defined the phase-change as the maximum difference in phase within 20 seconds before and after the phase-step.

When the particle is trapped, the phase-noise is comparable to the noise without a trapped particle. The measured phase thus gives some information about the initial dynamics of the trapping process, while the noise level must be reduced to get information about the subsequent propulsion along the waveguide. The phase change can be used to count how many particles are trapped on the waveguide. If many particles are trapped simultaneously, the phase changes will accumulate and the noise will probably increase, giving a maximum number of particles that can be counted.

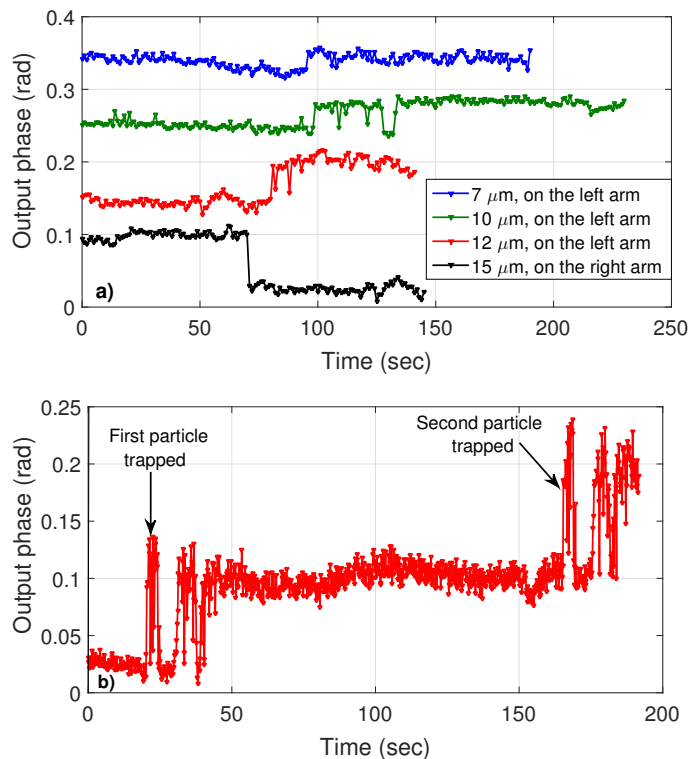


Fig. 6 a) Phase as a function of time for four trapping experiments with four different microparticle sizes. While the phase-step is positive for 7 μm , 10 μm and 12 μm particles, it is negative for the 15 μm particle. This is because the three smaller sizes were trapped on the left arm of the interferometer, while the 15 μm particle was trapped on the right arm. b) Phase when two particles of size 12 μm are trapped one after another.

To further explore the dependency of the phase change on particle size, the phase change was measured in five different measurements for each size, as shown in Fig. 7. All phase changes have been converted to negative values to give a graph that does not depend on trapping on left or right arm of the interferometer.

The phase change decreases with particle size, while the spread in the measured values increases. The simulated phase change is also shown in Fig. 7. For small spheres, approximately $7 \mu\text{m}$ diameter and less, the simulated phase change is a linear function of diameter. For larger spheres, morphology-dependent resonances (MDRs) start to appear, becoming very large for $15 \mu\text{m}$ diameter spheres. As the MDRs are sharp and closely spaced for the larger particles, it would require a large amount of simulations to resolve all the resonances by calculating the phase-change for very small changes in the particle diameter. Only three resonances are fully resolved in Fig. 7, and the graph thus gives upper and lower limits for the phase-change, rather than all the values.

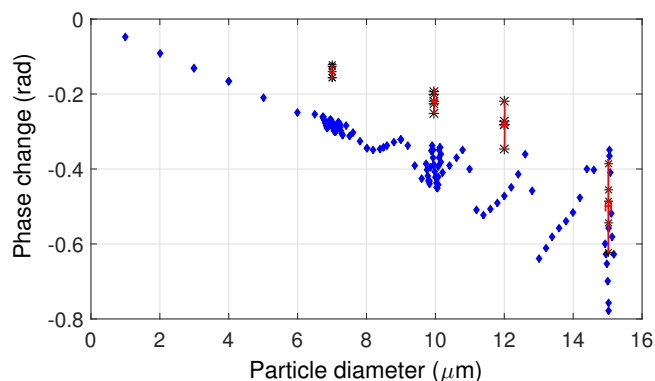


Fig. 7 Phase change as function of the particle diameter. Five measurements are shown for each particle size.

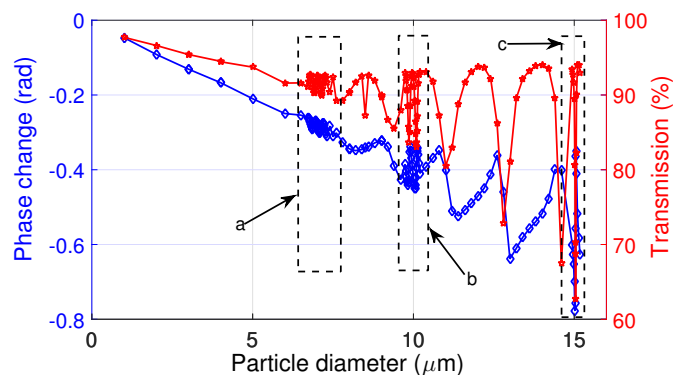


Fig. 8 Simulated phase change and transmission as function of the particle diameter. Note that the resonances are not fully resolved and the inserted lines are thus only guides to the eye. The three rectangular boxes (a, b, c) indicate parts that are given with full resolution in Fig. 9.

The simulated phase change is shown in Fig. 8 together with the simulated transmission due to trapping of particles. The curves for phase and transmission are similar in shape, and it is necessary to know the noise-level for each of them to determine if phase or transmission is best to measure the trapping of particles. For three resonances, for diameters of 7 , 10 and $15 \mu\text{m}$, the simulations have been done sufficiently closely to resolve one or a few resonances, see Fig. 9. For $7 \mu\text{m}$, the resonances cause a sinusoidal-like variation in phase and amplitude, for $10 \mu\text{m}$ the resonances are sharper and for $15 \mu\text{m}$ the typical shape of a res-

onance can be recognized, with a sharp dip in amplitude and its derivative for phase.

Regarding the particles used experimentally, they have a small size-variation as indicated at the bottom of Fig. 9. For the smaller particles, the variation is smaller than the spacing between the MDRs. For $15 \mu\text{m}$ spheres, the variation is larger in absolute terms and the resonance peaks are sharper, and it is thus possible that some of the five particles have a diameter giving resonance while others are off resonance. This may explain the larger variation in the measured phase change for the larger particles.

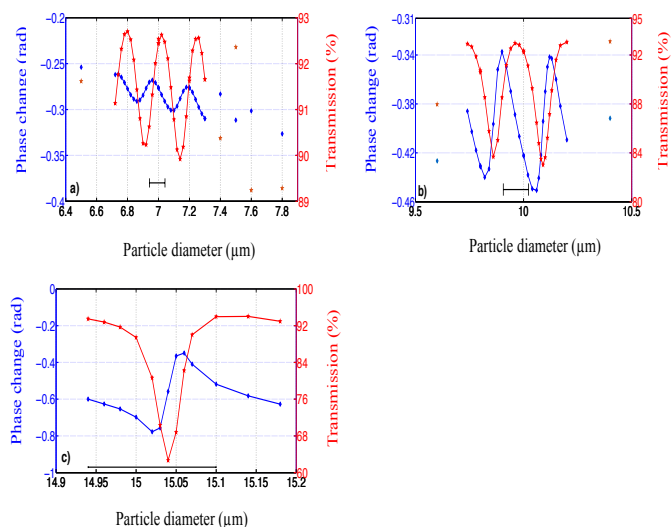


Fig. 9 Simulated phase change and transmission for trapping of particles exhibiting resonances (MDRs). Resonances are weak for a) $7 \mu\text{m}$ diameter, sharper for b) $10 \mu\text{m}$ and the typical shape of a resonance with high Q-value is shown for c) $15 \mu\text{m}$ diameter. The variation in the diameter of the particles used experimentally is indicated by horizontal error-bars at the bottom of the plots (arbitrary vertical position).

There is a rather large discrepancy between the measured and the simulated phase change in Fig. 7. For particles with $7 \mu\text{m}$ diameter, the resonances have limited influence on the phase-change, as shown in Fig. 9a. We have thus chosen to explore the discrepancy between measurements and simulations further for $7 \mu\text{m}$ particles. As pointed out in the Simulation-section, the refractive index of the materials is not precisely determined. Changing the refractive index of the waveguide core from 2.05 to 1.9827, changed the simulated phase change from -0.28 to -0.29 rad. Furthermore, setting the refractive index of silica to 1.4702 instead of 1.4496, gave a phase change of -0.26 . These changes are thus small compared to the difference between simulation and measurement. Fig. 10 shows the dependency on the refractive index of the sphere, n_s . According to Mie-theory, the resonance condition for the sphere depend on the size-parameter $k_s r = 2\pi n_s r / \lambda_0$, with r the radius of the sphere²². For large values of n_s , resonances thus start to appear even for a $7 \mu\text{m}$ particle, similar to the resonances for diameter in Fig. 9. However, for values of n_s close to 1.59, the dependency is approximately linear. To conclude,

variations in diameter or refractive index is thus insufficient to explain the discrepancy between measurements and simulations for $7\ \mu\text{m}$ particles.

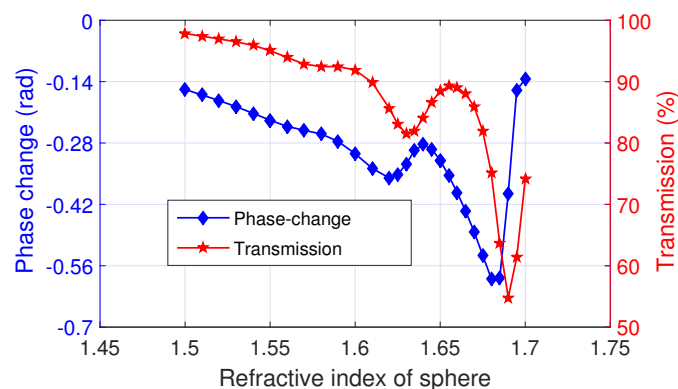


Fig. 10 Simulated phase change and transmission as function of refractive index n_s of the sphere.

The phase change depends on the position of the sphere relative to the centre of the waveguide and on the gap between the top of the waveguide and the bottom of the sphere, as shown in Fig. 11. The influence on the transmission is also shown. The simulated dependencies for phase change and transmission have the same shape, which resembles the mode profile of the waveguide. The measured phase change for a $7\ \mu\text{m}$ particle was $-0.13\ \text{rad}$. For the simulations to give the same value, the sphere must be displaced $1.4\ \mu\text{m}$ sideways (displacement in x , Fig. 11a) or there must be a gap of $85\ \text{nm}$ between the waveguide and the sphere (displacement in y , Fig. 11b). As the waveguide is $2\ \mu\text{m}$ wide, a lateral displacement of $1.4\ \mu\text{m}$ is highly unlikely, as this implies that the particle would be trapped and propelled forward with the centre of the particle completely off the waveguide. The evanescent field of the waveguide stretches some $200\ \text{nm}$ into the water, giving a strong downward force F_y that pulls the particle down towards the waveguide surface, as shown in Fig. 12. As the density of the polystyrene is close to that of water, gravitation will be balanced by buoyancy. As the particle is propelled forward, hydrodynamic forces will push the particle upwards from the surface. In addition, there are electrostatic forces between the surface and the sphere, in part due to the silanisation of the surface to get good adherence for PDMS. It is thus likely that there will be a gap between the waveguide surface and the bottom of the particle. However, further study is necessary to determine if the measured phase change is due to this gap.

Finally, we have simulated the vertical force F_y and the horizontal force F_z on the particle, as function of particle diameter, see Fig. 12. The forces are similar in shape to the phase-change and transmission in Fig. 8. Again, only three resonances are fully resolved. For the sharp resonance of a $15\ \mu\text{m}$ sphere, both F_y and F_z have maxima, which, as F_y is negative and F_z is positive, indicates a small downward force and a large forward propulsion force. This is consistent with the predictions of analytical Mie-theory²³. A positive F_y was predicted in²³, but does not appear in Fig. 12, probably because the coupling between the waveguide and the sphere was approximated in the analytical theory.

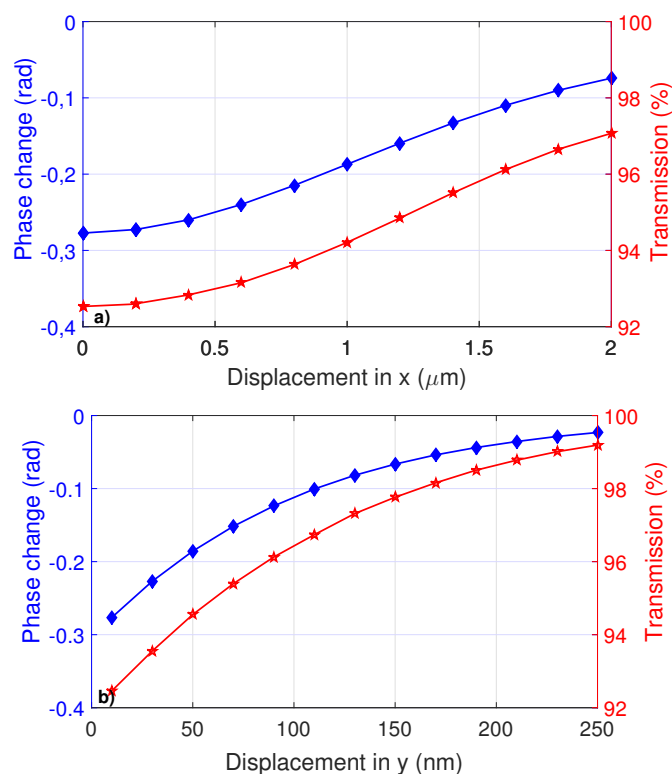


Fig. 11 Simulated change in phase and transmission for displacement in a) x and b) y of the particle relative to the centre of the waveguide surface. For displacement in y , the graph has an exponential shape as given by the decay of the evanescent field. Laterally, in x , the graph has a gaussian shape, with a width given by the half-width of the waveguide ($1\ \mu\text{m}$).

4 Conclusion

The phase-change due to trapping of microparticles has been measured and compared with simulations. The measured phase-change depends on the size of the particle, but for large particles, the phase change varies considerably for particles with the same diameter. According to the simulations, the (negative) phase change decreases with diameter up to approximately $7\ \mu\text{m}$ diameter. For larger diameters, morphology-dependent resonances (MDRs) start to appear and become dominant for $15\ \mu\text{m}$ diameter. Experimentally, variations in the diameter of nominally identical spheres can give resonance for some spheres and not for others, thus explaining the large variation in the measured phase-change for the large spheres.

For $7\ \mu\text{m}$ particles, there is a rather large discrepancy between the measured phase change of $-0.13\ \text{rad}$ and the simulated value of $-0.28\ \text{rad}$. We have looked into several factors that can influence the phase change. The refractive indices of the waveguide materials have a limited influence, while the phase change is approximately proportional to the refractive index of the particle up to a value giving MDRs. The phase change is influenced by the location of the sphere relative to the centre of the waveguide. Laterally, a displacement of $1.4\ \mu\text{m}$ would be necessary to explain the discrepancy between measured and simulated phase-change, which is not realistic as the waveguide has a half-width of $1\ \mu\text{m}$.

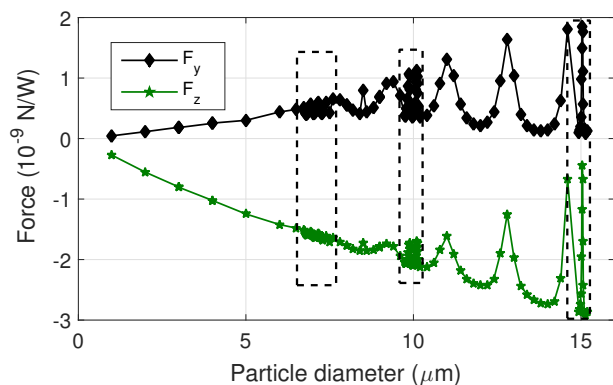


Fig. 12 Simulated forces as function of diameter of the sphere. The line is a guide to the eye, as the resonances are not resolved.

Vertically, a gap of 85 nm would be sufficient. This is also a rather large value, but there will be a balance between optical, electrostatic and hydrodynamic forces as the particle moves forward, giving a gap between the waveguide and the particle. To further investigate the phase change, it would be interesting to do hydrodynamic simulations, measure the velocity and do 3D-tracking of the particle during trapping. For 3D-tracking, off-focus imaging can be used²⁴, but it requires fluorescent particles and a high-magnification objective, e.g. 50x. The field-of-view would thus be reduced, making it necessary to use a shorter sensing window as it is necessary to see all trapped particles.

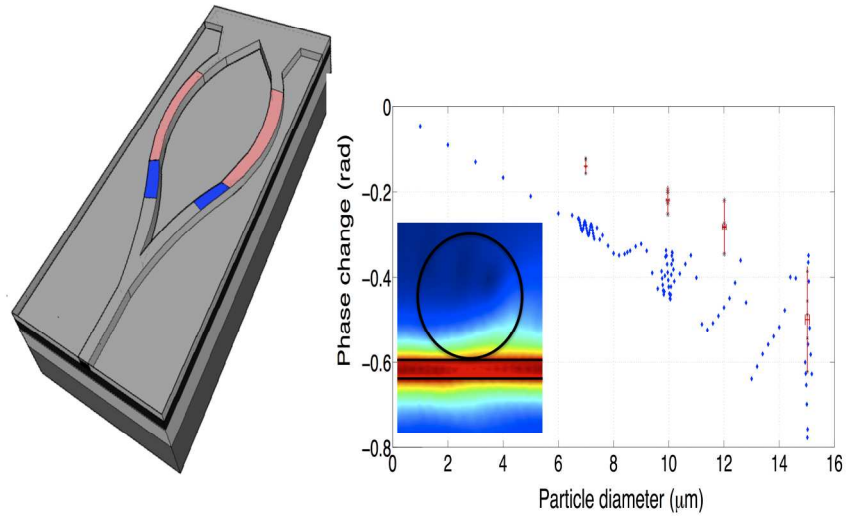
Trapping and propulsion of particles on the surface of a waveguide can be combined with functions for sorting and detection of particles, to become a lab-on-chip for nano- and microparticles. Measurement of phase change can be one of the building blocks in such a system. The sensing region can be as small as the particle size. It requires an interferometer, while detection of transmission can be done on any waveguide. However, we found that the noise is smaller for phase change than for transmission. A Young interferometer was used in this work, which makes it easy to split changes in phase from changes in amplitude, and it is convenient to use in a lab-setting. For a lab-on-chip, a Mach-Zehnder interferometer is probably preferable, as it requires only one or two detectors, as opposed to a camera or an array-detector for the Young interferometer.

5 Acknowledgment

This work was supported by the Research Council of Norway. The authors would like to thank Dr. B. S. Ahluwalia, Dr. Jana Jägerstätter and Øystein Ivar Helle for their valuable suggestions.

References

- 1 S. Kawata and T. Sugiura, *Optics Letters*, 1992, **17**, 772–774.
- 2 L. Ng, M. Zervas, J. Wilkinson and B. Luff, *Applied Physics Letters*, 2000, **76**, 1993–1995.
- 3 K. Grujic, O. Hellesø, J. Wilkinson and J. Hole, *Optics Communications*, 2004, **239**, 227–235.
- 4 S. Gaugiran, S. Gétin, J. Fedeli, G. Colas, A. Fuchs, F. Chate-lain and J. Dérourard, *Optics Express*, 2005, **13**, 6956–6963.
- 5 D. Néel, S. Gétin, P. Ferret, M. Rosina, J. Fedeli and O. Hellesø, *Applied Physics Letters*, 2009, **94**, 253115.
- 6 O. G. Hellesø, P. Løvhaugen, A. Z. Subramanian, J. S. Wilkin-son and B. S. Ahluwalia, *Lab on a Chip*, 2012, **12**, 3436–3440.
- 7 N. Descharmes, U. P. Dharanipathy, Z. Diao, M. Tonin and R. Houdré, *Physical Review Letters*, 2013, **110**, 123601.
- 8 P. Løvhaugen, B. S. Ahluwalia, T. R. Huser and O. G. Hellesø, *Optics Express*, 2013, **21**, 2964–2970.
- 9 M. Boerkamp, T. van Leest, J. Heldens, A. Leinse, M. Hoek-man, R. Heideman and J. Caro, *Optics Express*, 2014, **22**, 30528–30537.
- 10 P.-T. Lin, H.-Y. Chu, T.-W. Lu and P.-T. Lee, *Lab on a Chip*, 2014, **14**, 4647–4652.
- 11 S. A. Khan, Y. Shi, C.-M. Chang, C. Jan, S. Fan, A. K. Ellerbee and O. Solgaard, *Optics Express*, 2015, **23**, 8855–8866.
- 12 Ø. I. Helle, B. S. Ahluwalia and O. G. Hellesø, *Optics Express*, 2015, **23**, 6601–6612.
- 13 F. Prieto, B. Sepulveda, A. Calle, A. Llobera, C. Domínguez, A. Abad, A. Montoya and L. M. Lechuga, *Nanotechnology*, 2003, **14**, 907.
- 14 R. Bruck, E. Melnik, P. Muellner, R. Hainberger and M. Läm-merhofer, *Biosensors and Bioelectronics*, 2011, **26**, 3832–3837.
- 15 Q. Liu, X. Tu, K. W. Kim, J. S. Kee, Y. Shin, K. Han, Y.-J. Yoon, G.-Q. Lo and M. K. Park, *Sensors and Actuators B: Chemical*, 2013, **188**, 681–688.
- 16 I. S. Duport, P. Benech and R. Rimet, *Applied Optics*, 1994, **33**, 5954–5958.
- 17 P. Kozma, F. Kehl, E. Ehrentreich-Förster, C. Stamm and F. F. Bier, *Biosensors and Bioelectronics*, 2014, **58**, 287–307.
- 18 I. Malitson, *JOSA*, 1965, **55**, 1205–1208.
- 19 F. T. Dullo, J.-C. Tinguely, S. A. Solbø and O. G. Hellesø, *Pho-tonics Journal, IEEE*, 2015, **7**, 1–11.
- 20 L. Gao, F. Lemarchand and M. Lequime, *Journal of the Euro-pean Optical Society-Rapid publications*, 2013, **8**, year.
- 21 H. R. Philipp, *Journal of the Electrochemical Society*, 1973, **120**, 295–300.
- 22 X. Zheng and D. Carroll, *Journal of Optics A: Pure and Applied Optics*, 1999, **1**, 168.
- 23 H. Jaising, K. Grujić, O. G. Helles et al., *Optical Review*, 2005, **12**, 4–6.
- 24 M. Speidel, A. Jonáš and E.-L. Florin, *Optics Letters*, 2003, **28**, 69–71.



The phase change caused by microparticles trapped on a waveguide is simulated and measured using a Young interferometer.
209x148mm (300 x 300 DPI)